Revealing their true stripes: Mg/Ca banding in the Paleogene planktonic foraminifera genus *Morozovella* and implications for paleothermometry

Eleanor H. John[1], Philip T. Staudigel[1,2], Benjamin Buse[3], Caroline H. Lear[1], Paul N. Pearson[1], Sophie M. Slater[1]

[1]School of Earth and Environmental Sciences, Cardiff University, Main Building, Park Place, Cardiff, UK, CF10 3AT

[2]Institut für Geowissenschaften, Goethe-Universität Frankfurt, Frankfurt am Main, Germany

[3]School of Earth Sciences, University of Bristol, Wills Memorial Building, Bristol, UK, BS8 1RJ

Corresponding author: Eleanor H. John (johne11@cardiff.ac.uk, eleanor.h.john@gmail.com)

Key Points:

- Alternating bands of high and low Mg/Ca calcite are found throughout the tests of *Morozovella aragonensis* and *M. crater.*
- Intra-test Mg distributions in these species are similar to those in modern species upon which Mg/Ca-temperature calibrations are based.
- Our results support the use of EPMA in evaluating the preservation of fossil foraminifera.

ABSTRACT

The Mg/Ca ratio of foraminiferal calcite is a widely used empirical proxy for ocean temperature. Foraminiferal Mg/Ca-temperature relationships are based on extant species and are species-specific, introducing uncertainty when applying them to the fossil tests of extinct groups. Many modern species show remarkable heterogeneity in their intra-test Mg distributions, typically due to the presence of high Mg bands, which have a biological origin. Importantly, banding patterns differ between species, which could affect Mg/Ca-temperature relationships. Few studies have looked at intra-test variability in Mg/Ca ratios in extinct species of foraminifera, despite the obvious implications for paleothermometry. We used electron probe microanalysis (EPMA) to investigate intra-test Mg distributions in the fossil tests of two species of planktonic foraminifera from the extinct muricate mixed-layer-dwelling genus *Morozovella*, commonly used in Paleogene sea surface temperature reconstructions. Both *M. aragonensis* and *M. crater* show striking Mg banding patterns with multiple high and low Mg/Ca band pairs throughout the test wall in all chambers. The intra-test Mg variability in *M. aragonensis* and *M. crater* is similar to that in modern species widely used in paleoclimate reconstructions and banding patterns are consistent with published growth models for modern forms, albeit with subtle differences. The presence of Mg bands supports

This article has been accepted for publication and undergone full peer review but has not been through the copyediting, typesetting, pagination and proofreading process, which may lead to differences between this version and the Version of Record. Please cite this article as doi: 10.1029/2023PA004652.

the application of Mg/Ca-palaeothermometry in extinct *Morozovella* species as well as the utility of EPMA for examining preservation of foraminifera tests in paleoclimatological studies. However, we emphasize the importance of rigorous assessments of inter- and intra-test Mg variability when using microanalytical techniques for foraminiferal Mg/Ca paleothermometry.

Plain language summary

It is widely accepted that the incorporation of Mg into the calcium carbonate shells ('tests') of foraminifera (single-celled marine organisms) is dependent on temperature. As such, measurement of Mg/Ca ratios in fossil tests from deep-sea sediments has become an important working tool for reconstructing past seawater temperatures. However, Mg/Ca-temperature relationships are based on modern foraminifera and are species-specific, which introduces uncertainty when we apply them to extinct species. Furthermore, modern foraminifera tend to have distinct high Mg/Ca bands in their test walls and these bands are biologically controlled, with differences in banding patterns between species. Few studies have compared banding patterns in extinct foraminifera species with those in modern forms, despite the potential implications for the accuracy and precision of Mg/Ca paleotemperature reconstructions. We used electron probe microanalysis (EPMA) to investigate the distribution of Mg within the well-preserved fossil tests of two species belonging to the extinct mixed layer dwelling genus, *Morozovella*, which is commonly used in Paleogene (~66–23 million years ago) ocean temperature reconstructions. Our results show striking Mg banding patterns in *M. aragonensis* and *M. crater* similar to those described in modern species. Overall, our data support the use of these extinct species in Mg/Ca paleothermometry.

1. INTRODUCTION

1.1 Background

The Mg/Ca ratio of the calcite shells or 'tests' of planktonic foraminifera is widely used as a proxy for sea surface temperature (SST) and has been pivotal in improving our understanding of global paleoclimates. The Mg/Ca temperature proxy is particularly important as it seems to be less affected by diagenetic alteration than foraminiferal oxygen isotope ratios ($\delta^{18}O$) (Jonkers et al., 2012; Sexton et al., 2006; Staudigel et al., 2022). Empirical relationships between calcification temperature and test Mg/Ca values have been established for modern foraminifera based on bulk solution analytical techniques averaging multiple specimens (e.g. Anand et al., 2003; Dekens et al., 2002; Lea et al., 1999; Nürnberg et al., 1996). However, these relationships are species-specific due to strong and variable biological controls (collectively known as 'vital effects') on Mg incorporation

into the tests of different species (e.g. Bentov & Erez 2006; Jonkers et al., 2012; de Nooijer et al., 2014; Spero et al., 2015).

Studies at the micro- and nano-scale have revealed that Mg is not uniformly distributed within foraminifera tests, with distinct alternating high and low Mg/Ca bands in the test wall that cannot be explained by changes in external environmental factors such as temperature or pH (e.g. Eggins et al., 2004; Fehrenbacher & Martin 2014; Fehrenbacher et al., 2017; Jonkers et al., 2016; Sadekov et al., 2005; Spero et al., 2015). These bands have variably been attributed to changes in the composition of the calcifying fluid during chamber formation (Bentov & Erez 2006; Erez 2003; Jonkers et al., 2016; de Nooijer et al., 2014), the presence of organic membranes (Bonnin et al., 2019; Branson et al., 2016; Geerken et al., 2019; Kunioka et al., 2006), and/or diurnal oscillations in a) the pH of the foraminifer micro-environment due to changes in symbiont activity (Eggins et al., 2004) or b) mitochondrial sequestration of Mg (Spero et al., 2015). Importantly, banding patterns vary between species in term of the number, thickness, and arrangement of the high Mg/Ca bands and it has been hypothesized that this is responsible for inter-species variability in average elemental compositions. For example, the greater number and thickness of high Mg/Ca bands in specimens of *Orbulina universa* likely explains their overall higher test Mg/Ca concentrations and the higher pre-exponential factor in this species' Mg/Ca-temperature equation (Eggins et al., 2004; Sadekov et al., 2005; Spero et al., 2015).

There has also been an increased focus on using microanalytical techniques to measure Mg/Ca ratios in paleoclimate reconstructions, for example measurements of Mg/Ca ratios by electron probe micro-analysis (EPMA; Kozdon et al., 2011, 2013) or averages of Mg/Ca profiles measured across individual chamber walls using laser ablation inductively coupled mass spectrometry (LA-ICP-MS; e.g. Nairn et al., 2021). Such targeted measurements fundamentally rely on an understanding of how Mg is distributed within the test wall (e.g. Sadekov et al., 2008). For example, the supposed lack of high Mg/Ca bands in the final chambers of *Tribolatus sacculifer* compared with preceding chambers means that measurements based only on final chambers of this species could be skewed towards lower Mg/Ca values than bulk test averages (Rustic et al., 2021; Sadekov et al., 2005). Furthermore, standard chemical cleaning protocols prior to Mg/Ca analysis (Barker et al., 2003) may result in the preferential dissolution of high Mg/Ca portions of the test, skewing Mg/Ca measurements to different degrees in different species. As such, an understanding of inter-species differences in Mg banding patterns is central to the application of the Mg/Ca-temperature proxy.

Studies investigating intra-test heterogeneity in Mg/Ca ratios are nearly all based on modern species. This presents uncertainty regarding the use of extinct species in paleoceanographic reconstructions. In other words, if we do not know that Mg banding patterns (and therefore, the influence of biologically controlled Mg in the sample) in extinct species are similar to those in extant species, it is difficult to assess the applicability of modern

Mg/Ca temperature equations. Further, banding patterns provide valuable insights into the underlying mechanisms of test formation and biomineralization processes in different foraminifera species; therefore, a better understanding of intra-test Mg distributions in non-extant species would allow us to assess similarities between them and their modern counterparts, which would ultimately help workers determine their reliability as proxy archives (Hollis et al., 2019). Detailed baseline knowledge about primary intra-test Mg/Ca patterns in extinct species would also enable us to assess the extent to which test Mg/Ca has been altered by diagenetic processes. This is pertinent as recent work has suggested that recrystallized foraminifera that display relict Mg banding may retain bulk test Mg/Ca values even as $\delta^{18}O$ values are reset (Staudigel et al., 2022). Importantly, this implies that Mg/Ca temperature records from some sites previously rejected on preservation grounds may be resurrected in the future, improving the spatial resolution of SST datasets.

In this study, we used electron probe micro-analysis (EPMA) maps to investigate the distribution of Mg in the tests of two Eocene species of planktonic foraminifera from the extinct Paleogene genus *Morozovella*. Morozovellids belong to a group of now-extinct 'muricate'-walled planktonic foraminifera that often dominate Paleogene foraminifera assemblages and are commonly used in paleoceanographic reconstructions over intervals of great interest to paleoclimatologists (e.g. the Paleocene-Eocene Thermal Maximum, the Early Eocene Climatic Optimum) (Anagnostou et al., 2016; Boersma et al., 1987; Edgar et al., 2007; Evans et al., 2016; Henehan et al., 2020; Zachos et al., 2007). Multi-species stable isotope and trace element analysis show that morozovellids lived in the upper ocean (Anagnostou et al., 2016; John et al., 2013; Pearson et al., 2001, 2007) and carbon isotope analysis shows they hosted algal photosymbionts like many modern species (D'Hondt et al., 1994; Luciani et al., 2017; Norris, 1996). However, morozovellids show visible differences to extant forms: for example, their 'muricate' test morphology ('muricae' = distinct calcite protrusions containing spine-like structures; Fig 1, S1) (Blow, 1979; Pearson et al., 2022) is not found today, thus challenging analogies with modern species upon which Mg/Ca-temperature calibrations are based. We focused on *M. aragonensis* and *M. crater*, two common morozovellids from the early–middle Eocene. This work expands on that of Bhatia . (2019) who first reported banding in Eocene morozovellids. To ensure we were examining primary features, we used fossils from the Kilwa Group of Tanzania (Nicholas et al., 2006), known for the exceptional 'glassy' preservation of foraminifera within its sediments (Pearson et al., 2001, 2007; Sexton et al., 2006). We also used EPMA to visualize potential differences in intra-test Mg heterogeneity in poorly preserved morozovellid fossils from two deep-sea drilling sites with different diagenetic histories.

The overall aims of this study were to 1) describe Mg/Ca heterogeneity within the tests of *M. aragonensis* and *M. crater* as a reference for present and future comparisons with modern species, and 2) discuss the relevance for Mg-paleothermometry using these extinct species. Our results support the use of morozovellids for Mg

paleothermometry but highlight the importance of rigorous assessments of intra-test and inter-test variability in Mg/Ca ratios when applying microanalytical techniques to this proxy.

1.2 Foraminifera test structure

The basic pattern of layering within a foraminifer test and the terminology used in this manuscript to describe aspects of test structure and growth are shown in Figure 2. In brief, the tests of planktonic foraminifera consist of multiple calcite chambers, which are added in succession as the foraminifera grows. In the classic growth model (Reiss, 1957), each chamber initially consists of a bilamellar unit, made up of an inner ('primary') calcite layer and an outer ('secondary') calcite layer. These two layers form either side of an organic layer called the primary organic sheet (POS) (Erez, 2003), also referred to as the primary organic membrane (POM). As each chamber forms, the secondary layer (but not the POS) covers the test, attaching the newly formed chamber to pre-existing chambers. This explains the progressive decrease in test thickness through successive chambers in the direction of growth and the layered structure of most foraminiferal tests. In this classic model, however, only two layers should be present in the final chambers of the test whereas some species, including the extant species *O. universa* (Eggins et al., 2004; Spero et al., 2015) and *Neogloboquadrina dutertrei* (Fehrenbacher et al., 2017), have many more layers in their final chambers. Based on these observations and the presence of multiple laminae in the final chambers of the extinct muricate genera *Morozovella* and *Acarinina*, Pearson et al. (2022) adapted the classic model to include multiple 'adult' layers, which are precipitated after the formation of the final chamber and are typically thinner than the primary and secondary layers (Fig. 2). Like the secondary layers, these adult layers also extend over the pre-existing test adding to the number of laminae seen in preceding chambers. At the end of the life cycle of many species of foraminifera, a special adult layer of gametogenic calcite (often forming a 'crust') is deposited over the entire test.

2. MATERIALS AND METHODS

For the main part of this study, we used foraminifera extracted from clay-rich material from Tanzania Drilling Project (TDP) Site 20 (UTM 37L; 555457 9013846; Nicholas et al., 2006) dated as earliest middle Eocene (Table S1). Sediments were soaked in water, gently disaggregated, and sieved to extract the > 63 µm fraction. Fossil tests of *M. aragonensis* and *M. crater* were picked from the 300–355 µm and 355–425 µm size fractions based on species descriptions in Berggren and Pearson (2006; Fig. 1). We also selected morozovellid specimens from early Eocene sediments from DSDP Site 527 (Walvis Ridge, southeast Atlantic; 28°02.49'S; 01°45.80'E) and ODP Site 865 (northeast Pacific; 18°26'N, 179°33'W) to examine Mg distributions in specimens known to have undergone microstructural reorganization during diagenesis. Scanning electron microscope (SEM) images of selected whole tests and shell fragments were taken before analysis using a FEI XL30 Field Emission Gun Environmental SEM

(ESEM) at Cardiff University, UK. SEM images of test wall cross sections in samples from TDP 20 show original calcite microstructure while morozovellids from DSDP Site 527 and ODP Site 865 show clear evidence of recrystallization (Fig. S1).

2.2 Electron Probe Microanalysis (EPMA)

Tests were briefly ultrasonicated in methanol and deionized water and then embedded in 25 mm blocks of Epothin^{TM}2 epoxy resin. Resin blocks were left to cure at room temperature for at least 7 days and then sanded and polished to expose the cross section of the test walls. Polished resin blocks were then coated with Ag to minimize beam damage (Smith 1986). A small number of samples and standards were coated at the same time in a Quorum Q150RS sputter coater (Quorum Technologies, Laughton, UK). Differences in sample height and distance to the target were minimized to ensure the same coat thickness on the standard and the unknown (Jurek et al., 1994; Matthews, 2019).

Elemental concentrations (incl. Mg, Ca) within target areas were measured using quantitative X-ray mapping on a JEOL 8530F field-emission electron microprobe equipped with 5 wavelength dispersive spectrometers (WDS) at the University of Bristol, UK. Spectrometers, standards, and background offsets are given in Table S2. SEM images of each target area were taken before mapping. Mg was measured on both a TAPH and TAP spectrometer to increase analytical sensitivity. Standards were calibrated at 10 nA, with 10 seconds on peak and 5 seconds on each background position. Spot measurements were made on the foraminifera cross sections prior to mapping to provide data for background correction. Mg was measured in differential mode to suppress the 3rd order Ca Kα and 2nd order Ca Kα respectively, which occur adjacent to the peaks being measured. The background height was determined from the spot analyses. Spot measurements were made at 5 nA using either a 5 or 10 µm diameter beam and the count times are given in Table S3. Sample areas were mapped at 15 kV and 80 nA using a focused beam, and the pixel size was 0.9 µm with a 500 ms dwell time. Two additional maps were generated from our TDP samples using the same parameters but with 0.4 µm pixel size to produce higher resolution images. Fe and Sr were also measured but this data is not presented here. Mn and Ag were measured on analytical points but not mapped; the latter was measured to check coat thickness.

The maps were exported as .csv files and python scripts were created to subtract the background intensity as determined from analytical points and to convert the files into a format for quantification in the Probe for EPMA software (Probe Software Inc, Eugene, US). The maps were quantified using the Armstrong phi-rho-z model (Armstrong, 1988). Pixels with less than 35% Ca were masked from further processing to omit non pure calcium carbonate pixels from analysis and remove edge effects. ImageJ software was used to generate Mg/Ca maps in mmol/mol. The detection limit for Mg for an average of 4 pixels is 0.015 wt% (or 1 pixel = 0.031 wt%) to 3 s.d.. Analytical uncertainty at 4 mmol/mol (close to the average map value) for an average of 4 pixels is ~ 9.5% S.E. By

averaging 8 pixels, this drops to 6%. For Mg/Ca ratios around 2 mmol/mol, 11 pixels need to be integrated to achieve an error of 10%. Note that the actual Mg/Ca ratios of each pixel will be subject to averaging with nearby material.

The target areas for our TDP maps (well-preserved foraminifera) included a thin, later-formed part of the test wall (ideally the final chamber), an area where muricae are concentrated so we could examine their internal structure, and a thicker inner part of the test that incorporated earlier growth. In two specimens, we examined up to 5 chambers through the same test to investigate systematic inter-chamber differences. We also mapped several chamber boundaries to investigate patterns of Mg/Ca banding during chamber formation. In total, thirty-one Mg/Ca maps were generated from our well-preserved TDP samples: 18 maps were generated from seven *M. aragonensis* tests and 13 maps were made from five *M. crater* specimens. Two additional maps were generated from a muricae-rich area in an *M. crater* test from DSDP Site 527 and an *M. aragonensis* test from ODP Site 865 (both poorly preserved).

Final maps from the well-preserved (TDP) specimens were processed statistically using a MATLAB™ code, to facilitate direct comparison between similar maps of extant foraminifera (e.g. Sadekov et al., 2005; Fehrenbacher & Martin, 2014). Either the whole Mg/Ca map or a subset 'region of interest' was selected for subsequent statistics. In the case of the latter, we chose regions that represent a particular chamber (so that map averages did not include data from more than one chamber) or that avoided evidence of contamination. The script then calculated the arithmetic mean, harmonic mean, standard deviation, kurtosis, and skew for all the selected pixels (>35 wt% Ca) within the target area. For most maps, a transect approximately perpendicular to the test wall was analyzed to illustrate the Mg/Ca fluctuations associated with banding in two dimensions.

2.2 ICP-MS

To make an inter-method comparison of Mg/Ca values, we analyzed Mg/Ca ratios in three of our samples (TDP 20 27-3 44-54 cm, ODP 865B 9-6 0-4 cm, DSDP 527* 18-4 76-80 cm) using inductively coupled plasma mass spectrometry (ICP-MS) as well as EPMA. In each, twenty to thirty tests of *M. aragonensis* were broken between glass plates, ultrasonicated, and inspected under the microscope so that impurities could then be removed with a wet paintbrush. Samples were prepared following the short (non-reductive) cleaning procedure outlined by Barker et al. (2003), dissolved, and analyzed for their trace elemental composition using a Thermo Scientific ELEMENT-XR HR-ICP-MS in the CELTIC facilities at Cardiff University, UK. Long term precision on Mg/Ca measurements was 0.7% (RSD).

3. RESULTS

The Mg/Ca maps of our well-preserved specimens (TDP) reveal striking banding patterns throughout the tests of all specimens of *M. aragonensis* and *M. crater*, with alternating bands of high and low Mg/Ca calcite parallel to the test surface (Figs 3, 4). Intra-test Mg/Ca values vary by as much as a factor of 10 (Figs 5, S2, S3), as seen in many modern species. The composition of the high Mg/Ca bands across individual chambers is generally more variable than the composition of the low Mg/Ca bands (Figs 5, S2, S3). The thickness of the high Mg/Ca bands varies from 1 to several μm although the wide bands in selected maps (e.g. Fig. 3c) could be an artefact of polishing obliquely to the bands and the lower bounds are limited by the 0.9 μm pixel size (bands thinner than this are not resolved in our maps). Mg banding is also present in the Mg intensity maps (Fig. S4) showing that Mg/Ca variations are not artefacts driven by changes in Ca concentrations.

The number of high Mg/Ca bands in the tests of *M. aragonensis* and *M. crater* decreases through successive chambers in the direction of growth: more bands are visible in the thicker chambers that include juvenile growth (up to 12 high Mg/Ca bands) relative to the thinner, late growth stage chambers (up to 7 high Mg/Ca bands in the final chambers) (Figs 3–5, S2, S3). However, the number of bands in the same whorl position (chamber 'number') is variable between different tests. There is no consistent trend towards higher or lower Mg/Ca values across the test walls, unlike in some modern species. The specimens examined in this study do not have well-developed gametogenic calcite crusts, which are typically un-banded and made of low Mg/Ca calcite, on the outer edge of the test (e.g. Eggins et al., 2003; Jonkers et al., 2016; Spero et al., 2015).

SEM images of polished test walls reveal distinct laminae, delineated by linear divisions parallel to the test surface (Figs 6, S1b, S5). In many (but not all) cases, each lamina contains both a high and a low Mg/Ca band, the former thinner than the latter. High Mg/Ca values appear to be mostly concentrated near the laminal boundaries but do also extend into the laminae themselves. It is not clear as to whether the high Mg/Ca values are consistently concentrated near the inner or outer edges of each lamina. At chamber boundaries we see that some bands (and laminae) are continuous between chambers, coating pre-existing test walls that are themselves also banded (Fig. S6). This supports the idea that both adult layers and secondary calcite layers cover pre-existing chambers, as in most published growth models (e.g. Erez 2003; Hemleben et al, 1989; Pearson et al., 2022). Unlike some modern species (e.g. *N. dutertrei*; Fehrenbacher et al., 2017), multiple bands of similar or greater thickness to those found in the final chambers are also seen in inner test areas (Fig. 3c, q). Interestingly, selected maps show how some Mg bands 'loop' around the edge of the test wall and taper off along the inside of the chamber (Figs 3f, m, 4k, l, S7). Mg bands also bend upward in places, away from the inner test wall (e.g. Fig. 3f, 4m); a discussion of how this relates to the muricate test structure is given in Section 4.3.

The statistics we compiled for each map or region of interest along with a corresponding histogram and transect are presented in Figures 5, S2, and S3. The area analyzed (if not the whole map) is shown as a red polygon

and the transect given as a red line between two points. Although a single EPMA map cannot be compared directly with multi-test solution analysis, the EPMA-derived Mg/Ca map averages for the TDP specimen represented by maps in Figure 3e–h are consistent with a bulk solution value measured using ICP-MS on the same species from the same sample. Note that the standard deviations in the former are much larger due to the high intra-test variability in Mg/Ca (4.26–4.82 ± 1.71–2.2 mmol/mol for EPMA map averages vs 4.77 ± 0.17 mmol/mol for bulk ICP-MS measurements, respectively, errors given as 1 s.d.). All maps show non-normal distributions of Mg/Ca with positive skewness (Fig. S2, S3). However, we still compared intra-test variability using first moment statistics for consistency with other studies (e.g. Fehrenbacher & Martin, 2014, Sadekov et al., 2005). Some extant species show significantly higher or lower Mg/Ca in the final chambers of their tests (Rustic et al., 2021; Sadekov et al., 2005, 2008), which means that the time spent in the adult phase and therefore the size of the final chamber may skew test Mg/Ca averages. Our results show that mean chamber Mg/Ca values and standard deviations do vary within the same test, but there is no consistent trend through successive chambers in the direction of growth (Fig. S8). Sadekov et al. (2005) examined the difference between the arithmetic and harmonic means across the walls of different chambers in 8 species of modern planktonic foraminifera to investigate whether the presence of high Mg/Ca bands skewed map averages to higher values. In our study, whilst there was considerable variation in the arithmetic-harmonic mean differences between chambers, there was no consistent trend through the test (Fig. S8).

The Mg/Ca maps for the diagenetically altered specimens from DSDP Site 527 and ODP Site 865 (Fig. 7) show very different Mg distribution patterns to each other and to the TDP sample. There is weak banding present in the Mg/Ca map from ODP Site 865 (*M. aragonensis*; first published in Staudigel et al., 2022), suggesting that whilst the amplitude of intra-test variations has been reduced, there has not been wholesale reorganisation of test Mg. Conversely, the Mg/Ca map from DSDP 527 shows no evidence of banding at all, which, in accordance with the model predictions of Staudigel et al. (2022), suggests alteration of bulk Mg/Ca. We do not make a direct comparison of the El/Ca values measured at the two sites because of their different ages and paleolatitudes and a full exploration of the diagenetic processes at each site is beyond the scope of this study. However, this is the first time that an un-banded diagenetic end member has been presented using a method with proven ability to resolve Mg bands in morozovellids. (Note that the bulk measurements made on the samples from ODP Site 865 and DSDP Site 527 also agree with the EPMA map average for the same sample, within 1 s.d. error, as shown in the table in Fig. 7).

4. DISCUSSION

4.1 Origin of banding

This study reveals striking Mg banding patterns in two species of *Morozovella*, an extinct genus of foraminifera with a muricate test structure that is not seen in extant forms. Whilst there are subtle differences with modern species, the presence of high Mg/Ca bands suggests that the mechanisms that generated them were similar. The amplitude of variations in Mg/Ca across the test walls in *M. aragonensis* and *M. crater* is too large to have been driven by changes in ambient seawater temperature or pH during the lifetime of the organism and is consistent with a biological control: if temperature-driven, the observed intra-test differences in Mg/Ca values would require repeated changes of >20°C (e.g. using the calibration of Anand et al., 2003), which is clearly unreasonable. Whilst determining the exact origin of the bands is beyond the scope of this study, we discuss the possibilities based on observations in modern forms.

The origin of Mg banding in extant species is debated and appears to differ between species, consistent with observations that calcification mechanisms and physiological controls on foraminifera microenvironments also vary between species. In some modern foraminifera, a high Mg/Ca band is associated with the addition of a new chamber and has been attributed to changes in the composition of the calcifying fluid during chamber formation. De Nooijer et al. (2014) suggested that an injection of a small amount of seawater early in the development of a new chamber may result in a high Mg band on the inside of the test wall. Conversely, Jonkers et al. (2016) proposed that high Mg/Ca bands at the outer edges of newly formed chambers in *Neogloboquadrina pachyderma* reflect a decrease in the discrimination of Mg incorporation towards the end of chamber formation. It is possible that one of the high Mg/Ca bands in each chamber wall in *M. aragonensis* or *M. crater* is associated with chamber formation processes, but the presence of multiple additional bands through the test walls of all chambers (including in the final chamber) indicates that such mechanisms are not the only cause of banding in these species. There is neither a gradual change in Mg/Ca values across test walls, nor a gradual change in Mg/Ca values towards the outside of each individual laminae (as seen in some benthic species e.g. Geerken et al., 2019), suggesting no gradual change in Mg discrimination during chamber/laminae formation, for example through Rayleigh fractionation (Figs 5, S2, S3).

Different authors have variably associated high or low Mg/Ca bands with organic layers, with different proposed mechanisms for Mg incorporation or discrimination (Bonnin et al., 2019; Branson et al., 2016; Eggins et al., 2004; Erez 2003; Geerken et al., 2019; Kunioka et al., 2006; Sadekov et al., 2005; Spero et al., 2015). Erez (2003) suggested that the different Mg/Ca compositions of bands seen in the test walls of the benthic species *Amphistegina lobifera* were due to different calcification pathways, with a high-Mg primary layer sourced from Ca-Mg-P-rich granules associated with the POS and low-Mg secondary layers sourced from vacuolized seawater on the outer side of the POS. Our data does not support the idea of individual laminae having either a low- or high-Mg composition but rather that most laminae include at least one high-low Mg/Ca band pair. Kunioka et al.

(2006) attribute high Mg/Ca bands to the presence of protein-bound Mg in organic layers in the modern planktonic species *Pulleniatina obliquiloculata*. Conversely, others have shown that organic layers in multiple species are instead associated with low Mg/Ca values (Eggins et al., 2004; Sadekov et al., 2005; Spero et al., 2015). More recent work by Branson et al. (2016) and Bonnin et al. (2019) on the nanometre scale provides strong evidence that the POS in *O. universa* (and *O. bilobata*) is enriched in Mg, contributing to intra-test Mg heterogeneity. However, these authors also reveal that not all Mg bands are hosted in organic templates, as also seen in the study by Branson et al., (2013), which demonstrated that Mg in bands in *O. universa* and *Amphestigina lessoni* is not hosted in organic molecules or in mineral interstices but is uniformly coordinated within the calcite mineral lattice. Whilst we cannot rule out an association between organic layers (particularly the POS) and Mg bands observed in this study, especially as many of the bands are next to laminal boundaries where organic layers were possibly once located, we deem it unlikely that organics can explain all Mg bands.

Experiments have shown that cultured specimens of *O. universa* (Spero et al., 2015) and *N. dutertrei* (Fehrenbacher et al., 2017) deposit multiple layers and Mg band pairs in day-night cycles after the formation of their final chambers, with thin layers of high Mg/Ca calcite deposited at night and thick layers of low Mg/Ca calcite deposited during the day. Mg banding in these modern species has been attributed to diurnal changes in a) the pH of the foraminiferal micro-environment due to day-night changes in symbiont activity (e.g. Bhatia et al., 2019; Eggins et al., 2004; Jørgensen et al., 1985; Kohler-Rink & Kühl, 2005; Rink et al., 1998; Sadekov et al., 2005) and b) mitochondrial activity/density (Spero et al., 2015), both of which are assumed to affect Mg incorporation. The banding patterns in the final chambers of *M. aragonensis* and *M. crater* show a remarkable resemblance to those in *O. universa* and *N. dutertrei* relative to other species of extant foraminifera. For example, studies have only reported zero or one high Mg band in the final chambers of the modern symbiont-bearing planktonic foraminifera species *T. sacculifer*, *G. ruber*, and *G. conglobatus* (Fehrenbacher & Martin, 2014; Sadekov et al., 2005, 2008) whereas up to 7 high Mg bands have been reported from the final chambers of *O. universa* and *N. dutertrei* (Eggins et al., 2004; Fehrenbacher et al., 2017; Spero et al., 2015), a similar number to those observed in the final chambers of *M. aragonensis* and *M. crater*. We suggest therefore that the multiple band-pairs in muricate species are best explained by diurnal pacing. If so, this provides an interesting insight into the life cycle of these morozovellids in that it is possible to constrain how long the species lived in the adult phase, in this case up to one week. This makes a total lifespan of a lunar month likely, as seems to be the case in some modern species (Bijma et al., 1990).

4.2 Implications for paleothermometry

The apparent similarities between banding patterns in the final chambers of Eocene morozovellids and modern *O. universa* warrant attention given that *O. universa* is typically excluded from Mg/Ca-temperature

reconstructions as it has a very different Mg/Ca-temperature equation (higher pre-exponential calibration constant) than other species. However, there are distinct differences between the Mg distributions and test morphologies of *O. universa* versus *M. aragonensis* and *M. crater*. Firstly, the tests of morozovellids (and most planktonic species included in Mg/Ca-temperature calibrations) are composed of multiple chambers arranged in a trochospire, much like most planktonic symbiont-bearing foraminifera species. Conversely, the tests of *O. universa* consist of a) a smaller, inner test corresponding to juvenile growth comprised of multiple chambers arranged in a trochospire and, b) uniquely, a single, large, completely embracing spherical chamber that is secreted around the early-formed portion of the test once the organism reaches maturity. This sphere is much thicker than the earlier chambers and makes up the vast majority of test calcite and indeed contains most of the Mg/Ca bands (Eggins et al., 2004; Spero et al., 2015). Importantly, the intra-test Mg variability statistics appear to be quite different in *O. universa* than other extant species as well as the morozovellids studied here. Sadekov et al. (2005) report standard deviations across the test walls of *O. universa*, *Globigerinoides ruber*, and *T. sacculifer* of 3.74, 1.79, and 1.59–1.68 mmol/mol Mg/Ca, respectively, from laser ablation profile measurements in the same core-top sample. Our map averages and profiles give standards deviations of 1.3–2.3 mmol/mol, which are much more similar to the values from *G. ruber* and *T. sacculifer*. Whilst it is still possible that morozovellids had different calibrations to modern species, the similarity in intra-test Mg/Ca variability between morozovellids and species with 'typical' Mg/Ca-temperature calibrations is reassuring.

The use of microanalytical techniques (e.g. LA-ICP-MS, SIMS, nanoSIMS) in paleoclimatology to measure Mg/Ca in individual chambers of single or multiple foraminifer tests has expanded in recent decades. Some authors have proposed Mg/Ca-temperature calibrations for a particular chamber within a species (e.g. Dueñas-Bohórquez et al., 2011) whilst others have emphasised the advantages of microspatial analysis for avoiding diagenetically altered or contaminated parts of the foraminifer test (e.g. Kozdon et al., 2011, 2013; Hollis et al., 2012, 2015; Nairn et al., 2021). However, the observed large inter- and intra-test Mg/Ca variability in sample populations of individual foraminifera species means that a thorough assessment of the extent to which this affects the reproducibility of bulk test Mg/Ca is recommended (Nairn et al., 2021; Nürnberg, 1995; Sadekov et al., 2008). As with bulk solution analysis, it has been emphasized that analyses from multiple specimens are needed to bring sample variance down to levels that are meaningful for paleotemperature reconstructions. For example, Sadekov et al. (2008) reported large inter- and intra-test Mg/Ca variability in populations of *G. ruber* from a site in the east Indian Ocean and attributed this to a range of site-specific environmental factors, the presence of low and high Mg bands within the test, and variations in the arrangement and thickness of these bands in different chambers of the same test. They used power analysis to determine the number of LA-ICP-MS-derived transect means needed to bring down measurement error to meaningful levels of Mg/Ca precision and concluded that

profile means from at least 15 tests were needed to achieve a temperature uncertainty of 2°C (1 SE) at 28°C. The authors advise that this prescribed number of tests is likely site-specific and so rigorous assessment of the number of measurements needed should be carried out on a sample-by-sample basis. In our study, we do not have enough measurements from the same sample to assess inter-test variability within a sample population. However, given that morozovellid tests are clearly banded with respect to Mg and that a) the number and thickness of bands varies within individual tests and b) there is no consistent relationship between the number of bands and the position in the test whorl between different specimens, we advise that a similar approach to Sadekov et al. (2008) should be taken when using profile means (LA-ICP-MS) or targeted area means (e.g. EPMA) to generate Mg/Ca values from morozovellids for paleotemperature reconstructions. This is of course unless the worker is specifically investigating seasonal or depth habitat temperature extremes, in which case the lunar month lifespan estimate is an important consideration (e.g. Wit et al., 2010; Haarmann, et al., 2011; Laepple & Huybers, 2013).

4.3 Insights into morozovellid growth

Patterns of banding and layering in *M. aragonensis* and *M. crater* are consistent with some aspects of the classic growth models for multi-chambered perforate foraminifera of Reiss (1957) and Erez (2003). These models can explain the layered structure seen in our Mg/Ca maps (and SEM images) and the progressive decrease in test thickness and number of bands/laminae through successive chambers in the direction of growth, later chambers having been subjected to fewer 'coatings'. These classic growth models, however, likely better explain banding patterns in species that exhibit minimal banding in their final chambers (e.g. *G ruber*, *T. sacculifer*) as they predict that only two laminae should be present. The patterns of Mg banding and layering in *M. aragonensis* and *M. crater* support a modification of the classic growth model whereby, in some species, multiple thinner 'adult' layers, each layer consisting of a high/low Mg/Ca band pair, are deposited over the test after the organism reaches maturity (Pearson et al., 2022). This additional layering is also seen in *N. dutertrei* (Fehrenbacher et al., 2017) and *O. universa* (Eggins et al., 2004; Spero et al., 2015). However, unlike morozovellids, the majority of (or indeed all) resolved Mg/Ca bands in *N. dutertrei* (and perhaps *O. universa*, although very thin bands may be present in the inner chambers) appear to have formed after the formation of the final chamber, with only thinly calcified walls with no visible bands present before (Fehrenbacher et al., 2017). This is clearly not the case in *M. aragonensis* and *M. crater* as maps from chamber boundaries clearly show the presence of pre-existing band pairs in older chambers that are then coated by younger laminae (e.g. Fig. S6) and the presence of multiple bands within inner parts of the test (e.g. Fig. 3c,e,q). The banding patterns in *M. aragonensis* and *M. crater* therefore reveal some similarities and some differences with modern species in terms of test construction but are overall consistent with published growth models.

Another interesting feature revealed by some of the maps is how secondary/adult layers 'loop' around the test wall adjacent to the aperture and then taper off along the inner test wall (Figs 3f,m, 4k,l, S7). This shows that the organic membrane that formed the template for these layers would have originally wrapped around the chamber edge near the aperture and extended along the inner test wall over short distances. Our Mg/Ca maps also reveal the Mg distribution around the 'muricae' of the *Morozovella* test walls. In *M. aragonensis* and *M. crater* the muricae are clustered on the chamber shoulders around the umbilicus and round the periphery where a continuous row of them produces a rim or keel (called a muricocarina by Blow, 1979; Fig. 1). The name murica is derived from the Latin *murus* = wall, emphasizing that they are part of the primary test wall formed by upward mounding of successively added layers (Benjamini & Reiss, 1979; Blow, 1979; Hemleben & Olsson, 2006). Pearson et al. (2022) showed evidence that muricae typically contain a central rod made of a single calcite crystal that projects through the test layers, which onlap onto them. They suggested that these rods projected through the test surface in life, forming spines, which were analogous but not homologous with the so-called 'true spines' of various modern genera such as *Globigerina*, *Globigerinoides*, *Trilobatus* and *Orbulina* (see Fig. S9 for schematic). We cannot expect the spine structures themselves to be continuously resolved as they are typically only 1–2 µm in diameter (Pearson et al., 2022), but linear high Mg/Ca anomalies orthogonal to the test surface in some of our images (e.g. Figs 3f, 4a) may occasionally trace their path. The exact Mg distribution we see in our maps depends on where the polished surface dissects the muricae. Our maps appear to mostly reveal off-centre dissections of the muricae where bands and laminae bend upward from secondary layers with newer layers onlapping against them (Fig. S9; Pearson et al., 2022). This is relevant for paleothermometry as it sheds light on how morozovellids might have harboured symbionts within an external spine array very much like modern spinose species, strengthening the comparison of Paleogene mixed layer species to modern spinose species occupying the same realm (Pearson et al., 2022).

4.4 Diagenetic considerations

Mg/Ca values of the fossil calcite tests of planktonic foraminifera from deep-sea cores are a major source of SST information. However, much of the data from open ocean sites have been discredited as the foraminiferal calcite has been visually diagenetically altered through dissolution or recrystallization. Solid state diffusion has also been proposed as a significant process impacting oxygen isotope values, although this has been disputed (Bernard et al., 2017; Evans et al. 2018). The exquisite banding in the well-preserved Eocene foraminifera suggests that solid state diffusion is not a significant concern for Mg/Ca on these timescales.

Overall, the process of diagenetic recrystallization and how it affects the geochemistry of foraminifera tests is poorly understood. Recent work by Staudigel et al. (2022) suggests that recrystallization can occur within a diffusively-restricted regime, meaning that recrystallized foraminifera that display relict banding may retain bulk

test Mg/Ca values even as $\delta^{18}O$ values are reset. This implies Mg/Ca banding potentially could be used as a screening tool for retention of primary bulk Mg/Ca values (Staudigel et al., 2022). Excitingly, this opens up the possibility of obtaining Mg/Ca temperature records from previously rejected sites as long as Mg bands are retained. Indeed, the authors' model also predicts that pervasive diagenetic alteration may ultimately result in the loss of Mg banding and the alteration of primary bulk Mg/Ca values, although this had not yet been shown prior to this study.

Whilst an investigation into the complex processes involved in diagenetic alteration are beyond the scope of our work, our results mean that we can say with a greater degree of confidence that original morozovellid test walls were banded with respect to Mg and that any deviation from the patterns shown in this study suggest some internal reorganisation of test Mg. Furthermore, Mg/Ca maps from Early Eocene morozovellids from two deep-sea drilling sites with different burial histories and strong evidence of diagenetic alteration show for the first time that whilst Mg banding may be retained in some recrystallized specimens, it can eventually be lost, supporting the model predictions of Staudigel et al. (2022). Future work should investigate intra- and inter-test Mg variability in a wide range of diagenetic settings to better constrain the controls on alteration of primary Mg/Ca signatures.

5. CONCLUSIONS

Mg/Ca banding has been reported in many extant species of planktonic foraminifera used in Mg/Ca-temperature calculations. Any intra-test Mg variability is inherently incorporated in bulk Mg/Ca-temperature equations and studies have shown that Mg/Ca-temperature sensitivity in the calcite of the low and high Mg/Ca bands is similar (Sadekov et al., 2009; Spero et al., 2015). However, given that biological controls affect inter- and intra-species differences in banding patterns, intra-test heterogeneity has clear implications for Mg/Ca paleothermometry on the population and individual test level. Whilst we do not have a full understanding of biological controls on biomineralization and foraminiferal geochemistry in modern species, it is prudent to assess similarities and differences between species used in Mg/Ca-temperature equations and non-extant forms to which the equations are applied.

We characterized the distribution of Mg within well-preserved fossil tests of *Morozovella crater* and *M. aragonensis* using electron probe microanalysis (EPMA). The tests of both species are characterized by alternating pairs of high and low Mg/Ca calcite, like many extant species. The presence of multiple high Mg bands in the final chambers of *M. aragonensis* and *M. crater* suggests diurnally paced banding in the adult phase of the life cycle, as seen in the modern species *Orbulina universa* and *Neogloboquadrina dutertrei*. Banding patterns observed in *M. aragonensis* and *M. crater* are consistent with growth models for foraminifera tests that include the addition of multiple 'adult' layers after the formation of the final chamber. Whilst the availability of data precludes a

conclusive comparison with extant species, the shape of the Mg/Ca distributions in the test walls of *M. crater* and *M. aragonensis* is similar to species such as *Globigerinoides ruber* and *Trilobatus sacculifer*, which are commonly incorporated into Mg/Ca-temperature relationships. Our results support the use of morozovellids for Mg paleothermometry in that they are banded like most modern forms but highlight the importance of rigorous assessments of intra-test and inter-test variability in Mg/Ca ratios when applying microanalytical techniques to this proxy. This study also highlights the utility of EPMA as a tool for distinguishing between well- and poorly-preserved foraminifera tests in palaeoclimatological studies.

OPEN RESEARCH

A Supplementary Information document along with .tif files and Matlab™ scripts used for generating the statistical data in Figs 5, S2, and S3 are available at Zenodo.org (John, 2023).

ACKNOWLEDGMENTS

This work was funded by NERC grant NE/P019102/1 to CHL. Thanks to Duncan Muir at Cardiff University's Electron Microbeam facility for his assistance in generating SEM images. This is Cardiff EARTH CRediT Contribution 16.

REFERENCES (formatted using EndNote™ 20)

Anagnostou, E., John, E.H., Edgar, K.M., Foster, G.L., Ridgwell, A., Inglis, G.N., Pancost, R.D., Lunt, D.J. and Pearson, P.N. (2016) Changing atmospheric CO_2 concentration was the primary driver of early Cenozoic climate', Nature, 533(7603), 380-+, http://dx.doi.org/10.1038/nature17423.

Anand, P., Elderfield, H. and Conte, M.H. (2003) Calibration of Mg/Ca thermometry in planktonic foraminifera from a sediment trap time series, Paleoceanography, 18(2), http://dx.doi.org/Artn 105010.1029/2002pa000846.

Barker, S., Greaves, M. and Elderfield, H. (2003) A study of cleaning procedures used for foraminiferal Mg/Ca paleothermometry, Geochemistry Geophysics Geosystems, 4, http://dx.doi.org/Artn 840710.1029/2003gc000559.

Benjamini, C.R., Z. (1979) Wall-hispidity and -perforation in Eocene planktonic foraminifera, Micropaleontology, 25, 141–150.

Bentov, S. and Erez, J. (2006) Impact of biomineralization processes on the Mg content of foraminiferal shells: A biological perspective, Geochemistry Geophysics Geosystems, 7, http://dx.doi.org/Artn Q01p08 10.1029/2005gc001015.

Bernard, S., Daval, D., Ackerer, P., Pont, S. and Meibom, A. (2017) Burial-induced oxygen-isotope re-equilibration of fossil foraminifera explains ocean paleotemperature paradoxes, Nature Communications, 8, http://dx.doi.org/ARTN 113410.1038/s41467-017-01225-9.

Bhatia, Rehemat (2019) Geochemical signals in fossil planktonic foraminifera. Doctoral thesis (Ph.D), UCL (University College London). https://discovery.ucl.ac.uk/id/eprint/10070155/

Bijma, J., Erez, J. and Hemleben, C. (1990) Lunar and Semi-Lunar Reproductive-Cycles in Some Spinose Planktonic Foraminifers, Journal of Foraminiferal Research, 20(2), 117–127, http://dx.doi.org/DOI 10.2113/gsjfr.20.2.117.

Blow, W.H. (1979) The Cainozoic Globigerinida, Leiden.

Boersma, A., Silva, I.P. and Shackleton, N.J. (1987) Atlantic Eocene Planktonic Foraminiferal Paleohydrographic Indicators and Stable Isotope Paleoceanography, Paleoceanography, 2(3), 287–331, http://dx.doi.org/10.1029/PA002i003p00287.

Bonnin, E.A., Zhu, Z.H., Fehrenbacher, J.S., Russell, A.D., Honisch, B., Spero, H.J. and Gagnon, A.C. (2019) Submicron sodium banding in cultured planktic foraminifera shells, Geochimica Et Cosmochimica Acta, 253, 127–141, http://dx.doi.org/10.1016/j.gca.2019.03.024.

Branson, O., Redfern, S.A.T., Tyliszczak, T., Sadekov, A., Langer, G., Kimoto, K. and Elderfield, H. (2013) The

coordination of Mg in foraminiferal calcite, Earth and Planetary Science Letters, 383, 134–141, http://dx.doi.org/10.1016/j.epsl.2013.09.037.

Branson, O., Bonnin, E.A., Perea, D.E., Spero, H.J., Zhu, Z.H., Winters, M., Honisch, B., Russell, A.D., Fehrenbacher, J.S. and Gagnon, A.C. (2016) Nanometer-Scale Chemistry of a Calcite Biomineralization Template: Implications for Skeletal Composition and Nucleation, Proceedings of the National Academy of Sciences of the United States of America, 113(46), 12934–12939, http://dx.doi.org/10.1073/pnas.1522864113.

D'Hondt, S., Zachos, J.C., Schultz, G. (1994) Stable Isotopic Signals and Photosymbiosis in Late Paleocene Planktic Foraminifera, Palaeobiology, 20(3), 391–406.

de Nooijer, L.J., Spero, H.J., Erez, J., Bijma, J. and Reichart, G.J. (2014) Biomineralization in perforate foraminifera, Earth-Science Reviews, 135, 48-58, http://dx.doi.org/10.1016/j.earscirev.2014.03.013.

Dekens, P.S., Lea, D.W., Pak, D.K. and Spero, H.J. (2002) Core top calibration of Mg/Ca in tropical foraminifera: Refining paleotemperature estimation, Geochemistry Geophysics Geosystems, 3, http://dx.doi.org/Artn 102210.1029/2001gc000200.

Edgar, K.M., Wilson, P.A., Sexton, P.F. and Suganuma, Y. (2007) No extreme bipolar glaciation during the main Eocene calcite compensation shift, Nature, 448(7156), 908–911, http://dx.doi.org/10.1038/nature06053.

Eggins, S., De Deckker, P. and Marshall, J. (2003) Mg/Ca variation in planktonic foraminifera tests: implications for reconstructing palaeo-seawater temperature and habitat migration, Earth and Planetary Science Letters, 212(3-4), 291–306, http://dx.doi.org/10.1016/S0012-821x(03)00283-8.

Eggins, S.M., Sadekov, A. and De Deckker, P. (2004) Modulation and daily banding of Mg/Ca in *Orbulina universa* tests by symbiont photosynthesis and respiration: a complication for seawater thermometry?, Earth and Planetary Science Letters, 225(3–4), 411–419, http://dx.doi.org/10.1016/j.epsl.2004.06.019.

Erez, J. (2003) The source of ions for biomineralization in foraminifera and their implications for paleoceanographic proxies, Biomineralization, 54, 115–149, http://dx.doi.org/Doi 10.2113/0540115.

Evans, D., Wade, B.S., Henehan, M., Erez, J. and Muller, W. (2016) Revisiting carbonate chemistry controls on planktic foraminifera Mg/Ca: implications for sea surface temperature and hydrology shifts over the Paleocene Eocene Thermal Maximum and Eocene Oligocene transition, Climate of the Past, 12(4), 819–835, http://dx.doi.org/10.5194/cp-12-819-2016.

Evans, D., Badger, M.P.S., Foster, G.L., Henehan, M.J., Lear, C.H. and Zachos, J.C. (2018) No substantial long-term bias in the Cenozoic benthic foraminifera oxygen-isotope record, Nature Communications, 9, available: http://dx.doi.org/ARTN 287510.1038/s41467-018-05303-4.

Fehrenbacher, J.S. and Martin, P.A. (2014) Exploring the dissolution effect on the intrashell Mg/Ca variability of the planktic foraminifer *Globigerinoides ruber*, Paleoceanography, 29(9), 854–868, http://dx.doi.org/10.1002/2013pa002571.

Fehrenbacher, J.S., Russell, A.D., Davis, C.V., Gagnon, A.C., Spero, H.J., Cliff, J.B., Zhu, Z. and Martin, P. (2017) Link between light-triggered Mg-banding and chamber formation in the planktic foraminifera *Neogloboquadrina dutertrei*, Nature Communications, 8, http://dx.doi.org/ARTN 1544110.1038/ncomms15441.

Geerken, E., de Nooijer, L.J., Roepert, A., Polerecky, L., King, H.E. and Reichart, G.J. (2019) Element banding and organic linings within chamber walls of two benthic foraminifera, Scientific Reports, 9, http://dx.doi.org/ARTN 359810.1038/s41598-019-40298-y.

Haarmann, T., Hathorne, E.C., Mohtadi, M., Groeneveld, J., Kolling, M., Bickert, T. (2011) Mg/Ca ratios of single planktonic foraminifer shells and the potential to reconstruct the thermal seasonality of the water column, Paleoceanography 26, PA3218.

Hemleben, C., Spindler, M., and Anderson, O. R. (1989) Modern Planktonic Foraminifera, Springer, New York, 363 pp., 1989.

Henehan, M.J., Edgar, K.M., Foster, G.L., Penman, D.E., Hull, P.M., Greenop, R., Anagnostou, E. and Pearson, P.N. (2020) Revisiting the Middle Eocene Climatic Optimum "Carbon Cycle Conundrum" With New Estimates of Atmospheric pCO_2 From Boron Isotopes, Paleoceanography and Paleoclimatology, 35(6), http://dx.doi.org/UNSP e2019PA00371310.1029/2019PA003713.

=

Hollis, C. J., Taylor, K. W. T., Handley, L., Pancost, R. D., Huber, M., Creech, J., Hines, B., Crouch, E. M., Morgans, H. E. G., Crampton, J. S., Gibbs, S., Pearson, P., and Zachos, J. C. (2012) Early Paleogene temperature history of the Southwest Pacific Ocean: reconciling proxies and models, Earth Planet. Sc. Lett., 349–350, 53–66.

Hollis, C.J., Hines, B.R., Littler, K., Villasante-Marcos, V., Kulhanek, D.K., Strong, C.P., Zachos, J.C., Eggins, S.M., Northcote, L. and Phillips, A. (2015) The Paleocene-Eocene Thermal Maximum at DSDP Site 277, Campbell Plateau, southern Pacific Ocean, Climate of the Past, 11(7), 1009–1025, http://dx.doi.org/10.5194/cp-11-1009-2015.

Hollis, C.J., Jones, T.D., Anagnostou, E., Bijl, P.K., Cramwinckel, M.J., Cui, Y., Dickens, G.R., Edgar, K.M., Eley, Y., Evans, D., Foster, G.L., Frieling, J., Inglis, G.N., Kennedy, E.M., Kozdon, R., Lauretano, V., Lear, C.H., Littler, K., Lourens, L., Meckler, A.N., Naafs, B.D.A., Palike, H., Pancost, R.D., Pearson, P.N., Rohl, U., Royer, D.L., Salzmann, U., Schubert, B.A., Seebeck, H., Sluijs, A., Speijer, R.P., Stassen, P., Tierney, J., Tripati, A., Wade, B., Westerhold, T., Witkowski, C., Zachos, J.C., Zhang, Y.G., Huber, M. and Lunt, D.J. (2019) The DeepMIP

contribution to PMIP4: methodologies for selection, compilation and analysis of latest Paleocene and early Eocene climate proxy data, incorporating version 0.1 of the DeepMIP database, Geoscientific Model Development, 12(7), 3149–3206, http://dx.doi.org/10.5194/gmd-12-3149-2019.

John, E.H., Pearson, P.N., Coxall, H.K., Birch, H., Wade, B.S. and Foster, G.L. (2013) Warm ocean processes and carbon cycling in the Eocene, Philosophical Transactions of the Royal Society a-Mathematical Physical and Engineering Sciences, 371(2001), http://dx.doi.org/ARTN 2013009910.1098/rsta.2013.0099.

John, Eleanor H. (2023). Supplementary files for John et al. 2023 (Version 1) [Dataset]. Zenodo. https://doi.org/10.5281/zenodo.8228690.

Jonkers, L., Buse, B., Brummer, G.J.A. and Hall, I.R. (2016) Chamber formation leads to Mg/Ca banding in the planktonic foraminifer *Neogloboquadrina pachyderma*, Earth and Planetary Science Letters, 451, 177–184, http://dx.doi.org/10.1016/j.epsl.2016.07.030.

Jonkers, L., de Nooijer, L.J., Reichart, G.J., Zahn, R. and Brummer, G.J.A. (2012) Encrustation and trace element composition of *Neogloboquadrina dutertrei* assessed from single chamber analyses - implications for paleotemperature estimates, Biogeosciences, 9(11), 4851–4860, http://dx.doi.org/10.5194/bg-9-4851-2012.

Jørgensen, B.B., Erez, J., Revsbech, N.P., Cohen, Y. (1985) Symbiotic photosynthesis in a planktonic foraminiferan, *Globigerinoides sacculifer* (Brady), studied with microelectrodes, Limnology & Oceanography, 30(6), 1253–1267.

Jurek, K., Renner, O. and Krousky, E. (1994) The Role of Coating Densities in X-Ray-Microanalysis, Mikrochimica Acta, 114, 323–326, http://dx.doi.org/Doi 10.1007/Bf01244558.

Kozdon, R., Kelly, D.C., Kita, N.T., Fournelle, J.H. and Valley, J.W. (2011) Planktonic foraminiferal oxygen isotope analysis by ion microprobe technique suggests warm tropical sea surface temperatures during the Early Paleogene, Paleoceanography, 26, http://dx.doi.org/Artn Pa320610.1029/2010pa002056.

Kozdon, R., Kelly, D.C., Kitajima, K., Strickland, A., Fournelle, J.H. and Valley, J.W. (2013) In situ delta O-18 and Mg/Ca analyses of diagenetic and planktic foraminiferal calcite preserved in a deep-sea record of the Paleocene-Eocene thermal maximum, Paleoceanography, 28(3), 517–528, http://dx.doi.org/10.1002/palo.20048.

Kohler-Rink, S. and Kühl, M. (2005) The chemical microenvironment of the symbiotic planktonic foraminifer *Orbulina universa*, Marine Biology Research, 1(1), 68–78, http://dx.doi.org/10.1080/17451000510019015.

Kunioka, D., Shirai, K., Takahata, N., Sano, Y., Toyofuku, T. and Ujiie, Y. (2006) Microdistribution of Mg/Ca, Sr/Ca,

and Ba/Ca ratios in *Pulleniatina obliquiloculata* test by using a NanoSIMS: Implication for the vital effect mechanism, Geochemistry Geophysics Geosystems, 7, http://dx.doi.org/Artn Q12p2010.1029/2006gc001280.

Laepple, T., Huybers, P. (2013). Reconciling discrepancies between U^{k}_{37} and Mg/Ca reconstructions of Holocene marine temperature variability, Earth Planet. Sci. Lett. 375, 418–429.

Lea, D.W., Mashiotta, T.A. and Spero, H.J. (1999) Controls on magnesium and strontium uptake in planktonic foraminifera determined by live culturing, Geochimica Et Cosmochimica Acta, 63(16), 2369–2379, http://dx.doi.org/Doi 10.1016/S0016-7037(99)00197-0.

Luciani, V., D'Onofrio, R., Dickens, G.R. and Wade, B.S. (2017) Planktic foraminiferal response to early Eocene carbon cycle perturbations in the southeast Atlantic Ocean (ODP Site 1263), Global and Planetary Change, 158, 119–133, http://dx.doi.org/10.1016/j.gloplacha.2017.09.007.

Matthews, M.B. (2019) Electron Probe Microanalysis through Coated Oxidized Surfaces, Microscopy Microanalysis, 25, 1112–1129.

Moore, T. C , Jr., Rabinowitz, P. D., et al. (1984) Site 527. Initial Reports of the Deep Sea Drilling Project, 74, 237–306. doi:10.2973/dsdp.proc.74.104.1984

Nairn, M. G., Lear, C. H., Sosdian, S. M., Bailey, T. R., & Beavington-Penney, S. (2021). Tropical sea surface temperatures following the middle Miocene climate transition from laser ablation ICP-MS analysis of glassy foraminifera. Paleoceanography and Paleoclimatology, 36, e2020PA004165. https://doi.org/10.1029/2020PA004165

Nicholas, C.J., Pearson, P.N., Bown, P.R., Dunkley Jones, T., Huber, B.T., Karega, A., Lees, J.A., McMillan, I.K., O'Halloran, A., Singano, J.M. and Wade, B.S. (2006) Stratigraphy and sedimentology of the Upper Cretaceous to Paleogene Kilwa Group, southern coastal Tanzania, Journal of African Earth Sciences, 45(4–5), 431–466, http://dx.doi.org/10.1016/j.jafrearsci.2006.04.003.

Norris, R.D. (1996) Symbiosis as an evolutionary innovation in the radiation of Paleocene planktic foraminifera, Paleobiology, 22(4), 461–480, http://dx.doi.org/Doi 10.1017/S0094837300016468.

Nürnberg, D. (1995) Magnesium in the tests of *Neogloboquadrina pachyderma* sinistral from high northern and southern latitudes, Journal of Foraminiferal Research, 25(4), 350–368.

Nürnberg, D., Bijma, J. and Hemleben, C. (1996) Assessing the reliability of magnesium in foraminiferal calcite as a proxy for water mass temperatures, Geochimica Et Cosmochimica Acta, 60(5), 803–814, http://dx.doi.org/Doi 10.1016/0016-7037(95)00446-7.

Pearson, P.N., Ditchfield, P.W., Singano, J., Harcourt-Brown, K.G., Nicholas, C.J., Olsson, R.K., Shackleton, N.J. and Hall, M.A. (2001) Warm tropical sea surface temperatures in the Late Cretaceous and Eocene epochs, Nature, 414(6862), 470–470, http://dx.doi.org/Doi 10.1038/35106617.

Pearson, P.N., van Dongen, B.E., Nicholas, C.J., Pancost, R.D., Schouten, S., Singano, J.M. and Wade, B.S. (2007) Stable warm tropical climate through the Eocene Epoch, Geology, 35(3), 211–214, http://dx.doi.org/10.1130/G23175a.1.

Pearson, P.N., John, E., Wade, B.S., D'haenens, S. and Lear, C.H. (2022) Spine-like structures in Paleogene muricate planktonic foraminifera, Journal of Micropalaeontology, 41(2), 107–127, http://dx.doi.org/10.5194/jm-41-107-2022.

Reiss, Z. (1957) The Bilamellidea, nov. superfam. and remarks on Cretaceous globorotaliids, Contrib. Cushman Found. Foram. Res., 8, 127–145.

Rink, S., Bijma, J., Spero, H.J. (1998) Microsensor studies of photosynthesis and respiration in the symbiotic foraminifer *Orbulina universa*, *Marine Biology*, 131, 583–595.

Rustic, G.T., Polissar, P.J., Ravelo, A.C. and DeMenocal, P. (2021) Relationship between individual chamber and whole shell Mg/Ca ratios in *Trilobatus sacculifer* and implications for individual foraminifera palaeoceanographic reconstructions, Scientific Reports, 11(1), http://dx.doi.org/ARTN 46310.1038/s41598-020-80673-8.

Sadekov, A.Y., Eggins, S.M. and De Deckker, P. (2005) Characterization of Mg/Ca distributions in planktonic foraminifera species by electron microprobe mapping, Geochemistry Geophysics Geosystems, 6, http://dx.doi.org/Artn Q12p0610.1029/2005gc000973.

Sadekov, A., S. M. Eggins, P. De Deckker, and D. Kroon (2008). Uncertainties in seawater thermometry deriving from intratest and intertest Mg/Ca variability in *Globigerinoides ruber*, Paleoceanography, 23, PA1215, doi:10.1029/2007PA001452

Sadekov, A., Eggins, S.M., De Deckker, P., Ninnemann, U., Kuhnt, W. and Bassinot, F. (2009) Surface and subsurface seawater temperature reconstruction using Mg/Ca microanalysis of planktonic foraminifera *Globigerinoides ruber, Globigerinoides sacculifer*, and *Pulleniatina obliquiloculata*, Paleoceanography, 24, http://dx.doi.org/Artn Pa320110.1029/2008pa001664.

Sager, W.W, Winterer, E.L., Firther, J.V. et al. (1993) Site 865. Proceedings of the Ocean Drilling Program, Initial Reports vol. 143. College Station, TX (Ocean Drilling Program).

Sexton, P.F., Wilson, P.A. and Pearson, P.N. (2006) Microstructural and geochemical perspectives on planktic foraminiferal preservation: "Glassy'' versus "Frosty'', Geochemistry Geophysics Geosystems, 7, http://dx.doi.org/Artn Q12p1910.1029/2006gc001291.

Smith, M.P. (1986) Silver coating inhibits electron microprobe beam damage of carbonates, Journal of Sedimentary Research, 56, 560–561.

Spero, H.J., Eggins, S.M., Russell, A.D., Vetter, L., Kilburn, M.R. and Honisch, B. (2015) Timing and mechanism for intratest Mg/Ca variability in a living planktic foraminifer, Earth and Planetary Science Letters, 409, 32–42, http://dx.doi.org/10.1016/j.epsl.2014.10.030.

Staudigel, P.T., John, E.H., Buse, B. and Lear, C.H. (2022) Apparent preservation of primary foraminiferal Mg/Ca ratios and Mg-banding in recrystallized foraminifera, Geology, 50(7), 760–764, http://dx.doi.org/10.1130/G49984.1.

van Hinsbergen, D.J., de Groot, L.V., van Schaik, S.J., Spakman, W., Bijl, P.K., Sluijs, A., Langereis, C.G. and Brinkhuis, H. (2015) A Paleolatitude Calculator for Paleoclimate Studies, PLoS One, 10(6), e0126946, http://dx.doi.org/10.1371/journal.pone.0126946.

Wit, J.C., Reichart, G.J., Jung, S.J.A., Kroon, D. (2010) Approaches to unravel seasonal-ity in sea surface temperatures using paired single-specimen foraminiferal $\delta^{18}O$ and Mg/Ca analyses. Paleoceanography 25, PA4220.

Zachos, J.C., Bohaty, S.M., John, C.M., McCarren, H., Kelly, D.C. and Nielsen, T. (2007) The Palaeocene-Eocene carbon isotope excursion: constraints from individual shell planktonic foraminifer records, Philosophical Transactions of the Royal Society a-Mathematical Physical and Engineering Sciences, 365(1856), 1829–1842, http://dx.doi.org/10.1098/rsta.2007.2045.

Armstrong, J.T. (1988) Quantitative analysis of silicate and oxide materials: comparison of Monte Carlo, ZAF, and phi-rho-z procedures. Microbeam Analysis, 239–246.

Dueñas-Bohórquez, A., da Rocha, R.E., Kuroyanagi, A., de Nooijer, L.J., Bijma, J. and Reichart, G.J. (2011) Interindividual variability and ontogenetic effects on Mg and Sr incorporation in the planktonic foraminifer Globigerinoides sacculifer, Geochimica Et Cosmochimica Acta, 75(2), 520-532, http://dx.doi.org/10.1016/j.gca.2010.10.006.

Hemleben, C. and Olsson, R.K. (2006) Wall textures of Eocene planktonic foraminifera. In P.N. Pearson, R.K. Olsson, B.T. Huber, C. Hemleben, W.A. Berggren (Eds.), Atlas of Eocene Planktonic Foraminifera, Cushman Foundation for Foraminiferal Research, Special Publication 41, pp. 47–69.

References from Supporting Information:

Pearson, P.N. and Coxall, H.K. (2014) Origin of the Eocene Planktonic Foraminifer *Hantkenina* by Gradual Evolution, Palaeontology, 57(2), 243–267, http://dx.doi.org/10.1111/pala.12064.

Pearson, P.N., Nicholas, C.J., Singano, J.M., Bown, P.R., Coxall, H.K., van Dongen, B.E., Huber, B.T., Karega, A., Lees, J.A., Msaky, E., Pancost, R.D., Pearson, M. and Roberts, A.P. (2004) Paleogene and cretaceous sediment cores from the Kilwa and Lindi areas of coastal Tanzania: Tanzania Drilling Project Sites 1-5, Journal of African Earth Sciences, 39(1-2), 25–62, http://dx.doi.org/10.1016/j.jafrearsci.2004.05.001.

Pearson, P.N., John, E., Wade, B.S., D'haenens, S. and Lear, C.H. (2022) Spine-like structures in Paleogene muricate planktonic foraminifera, Journal of Micropalaeontology, 41(2), 107–127, http://dx.doi.org/10.5194/jm-41-107-2022.

Nicholas, C.J., Pearson, P.N., Bown, P.R., Dunkley Jones, T., Huber, B.T., Karega, A., Lees, J.A., McMillan, I.K., O'Halloran, A., Singano, J.M. and Wade, B.S. (2006) Stratigraphy and sedimentology of the Upper Cretaceous to Paleogene Kilwa Group, southern coastal Tanzania, Journal of African Earth Sciences, 45(4-5), 431–466, http://dx.doi.org/10.1016/j.jafrearsci.2006.04.003.

Staudigel, P.T., John, E.H., Buse, B. and Lear, C.H. (2022) Apparent preservation of primary foraminiferal Mg/Ca ratios and Mg-banding in recrystallized foraminifera, Geology, 50(7), 760–764, http://dx.doi.org/10.1130/G49984.1.

Figure captions:

Figure 1. SEM images showing examples of sinistrally coiled *M. aragonensis* (a–c) and *M. crater* (d–f) specimens from sample TDP 20 27-1 0-10 cm. Images a) and f) show umbilical views, b) and e) show side views (revealing the aperture), and c) and f) show spiral views. Muricae occur over much of the ventral surface especially around the umbilicus (central depression). On the spiral side, muricae are concentrated along curving inter-cameral sutures and in the central region over the inner whorl. Muricae are also clustered round the test periphery where a continuous row of them produce a 'muricocarina'. Scale bars = 200 μm.

Figure 2. Equatorial cross section of a generic planktonic foraminifer showing the basic pattern of test layering (slightly modified from Pearson et al., 2022, itself modified from Reiss, 1957, Erez, 2003, and Fehrenbacher et al., 2017). Initial chamber formation consists of a bilamellar unit composed of a primary and secondary layer either side of a primary organic sheet (POS). The secondary layer(s) cover the entire external surface as each chamber is formed. Additional 'adult' layers, including a final gametogenic layer in some cases, are deposited at the end of the process.

Figure 3. Mg/Ca maps for multiple early middle Eocene *M. aragonensis* specimens from TDP Site 20. White boxes enclose maps made on the same specimen. Maps correspond to the following samples: a)–b) TDP 20 25-1 60—

70cm; c)–d) TDP 20 27-3 44-54cm; e)–h) TDP 20 27-3 44-54cm; i) TDP 20 core 29 (mixed samples); j)–m) TDP 20 26-2 90-100 300-355um Ma-1; n)–r) TDP 20 27-1 0-10cm. Foraminifera tests in a)–i) and n)–r) were taken from the >355 µm size fraction. Those in j)–m) were taken from the 300–355 µm size fraction. Wide high Mg/Ca bands in c) may be due to the polished surface being oblique to the orientation of the bands. The asterisks* denote maps/sections of maps from the final chamber of the foraminifer test. Maps b) and h), which both represent final chambers, appear not to correspond to areas on the SEM inset; this is because they were mapped after a re-polish and therefore removal of a small amount of surface material. All maps were generated with a resolution of 0.9 µm. Note the difference in Mg/Ca calibration bar for n)–r). Scale bars for maps denote 50 µm. Scale bars for SEM insets denote 100 µm. Map 1a has already been published in Staudigel et al. (2022).

Figure 4. Mg/Ca maps for early middle Eocene *M. crater* specimens from TDP 20. White boxes enclose maps made on the same specimen. a)–i) TDP 20 32-1 45-51cm; j)–m) TDP 20 30-1 45–51 cm. Tests in a)–k are taken from the >355 µm size fraction. l)–o) are taken from the 300–355 µm size fraction. The asterisks* mark final chambers. All maps were generated using a pixel size of 0.9 µm except for maps a) and b), which were made with a resolution of 0.4 µm. Scale bars for maps denote 50 µm. Scale bars for SEM insets denote 100 µm.

Figure 5. Frequency histograms (with statistics) and transects for selected EPMA maps (see Figs S2 and S3 for more) generated using MATLAB™ code. Reference EPMA maps are shown in the left-hand panels. The transects in the right-hand panel are shown with a weighted mean regression, which is calculated using the same normally distributed weighted mean approach used by Staudigel et al. (2022), with a kernel of 0.5 µm. The 95% confidence interval for this smoothed mean function is shown as a shaded region behind the data. The transects display the data from ±2 µm either side of a line defined by two points across a test wall (shown in the left hand EPMA map panels). Scale bars on Mg/Ca maps are 50 µm.

Figure 6. Mg/Ca maps from Fig. 3a (a) and c (b), respectively, with accompanying SEM images that show the relationship between laminae in the test wall and Mg/Ca banding. Additional comparisons are shown in Fig. S5. Scale bars for Mg/Ca maps and large images denote 50 µm. Scale bars for SEM insets denote 100 µm.

Figure 7. EPMA-derived Mg/Ca maps for a *M. crater* specimen from DSDP Site 527 and an *M. aragonensis* specimen from ODP Site 865 dated as early Eocene. The 527 specimen shows no evidence of Mg/Ca banding and evidence of dissolution in the SEM image inset. The 865 specimen shows evidence of relict banding and was first published in Staudigel et al. (2022). Scale bars are 50 µm. The table presents descriptions of samples from each

site (Moore et al., 1984; Sager et al., 1993) and Mg/Ca ratios measured by EPMA (map averages for each specimen) and ICP-MS measurements (on multiple specimens from each sample). *Paleolatitudes are calculated using the paleolatitude calculator of van Hinsbergen et al. (2015).

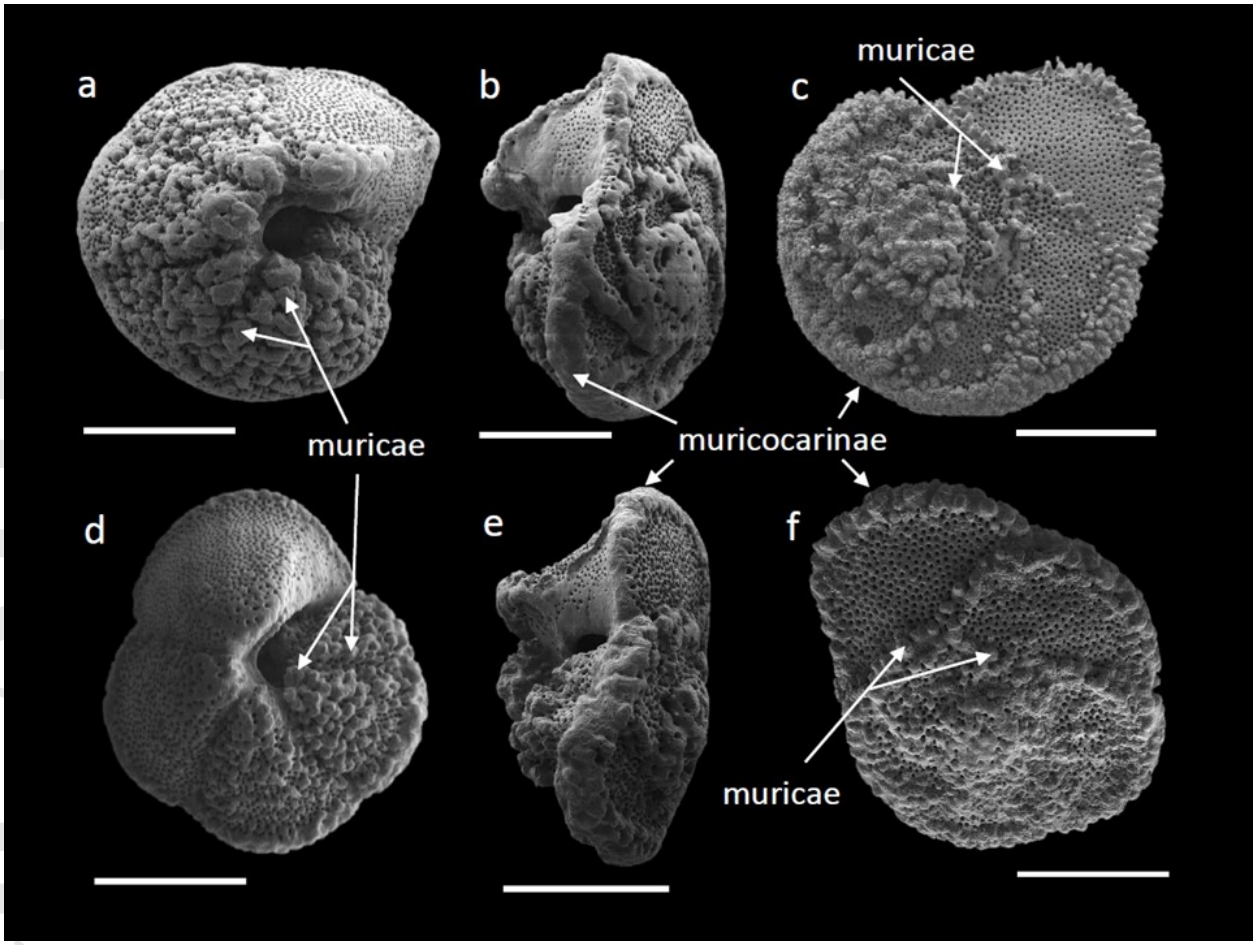

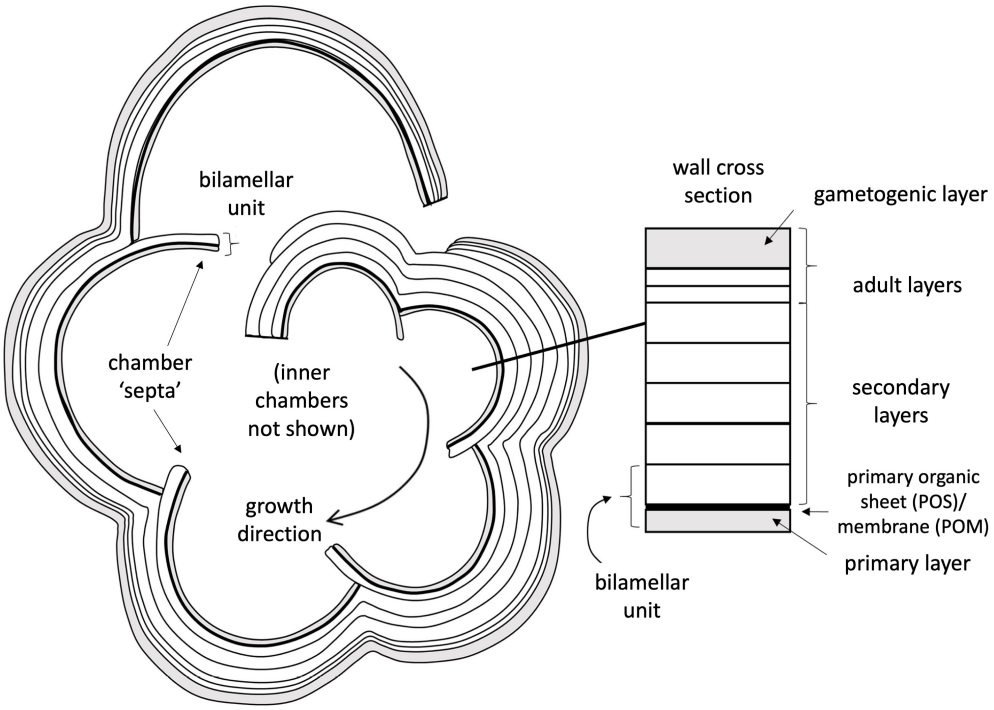

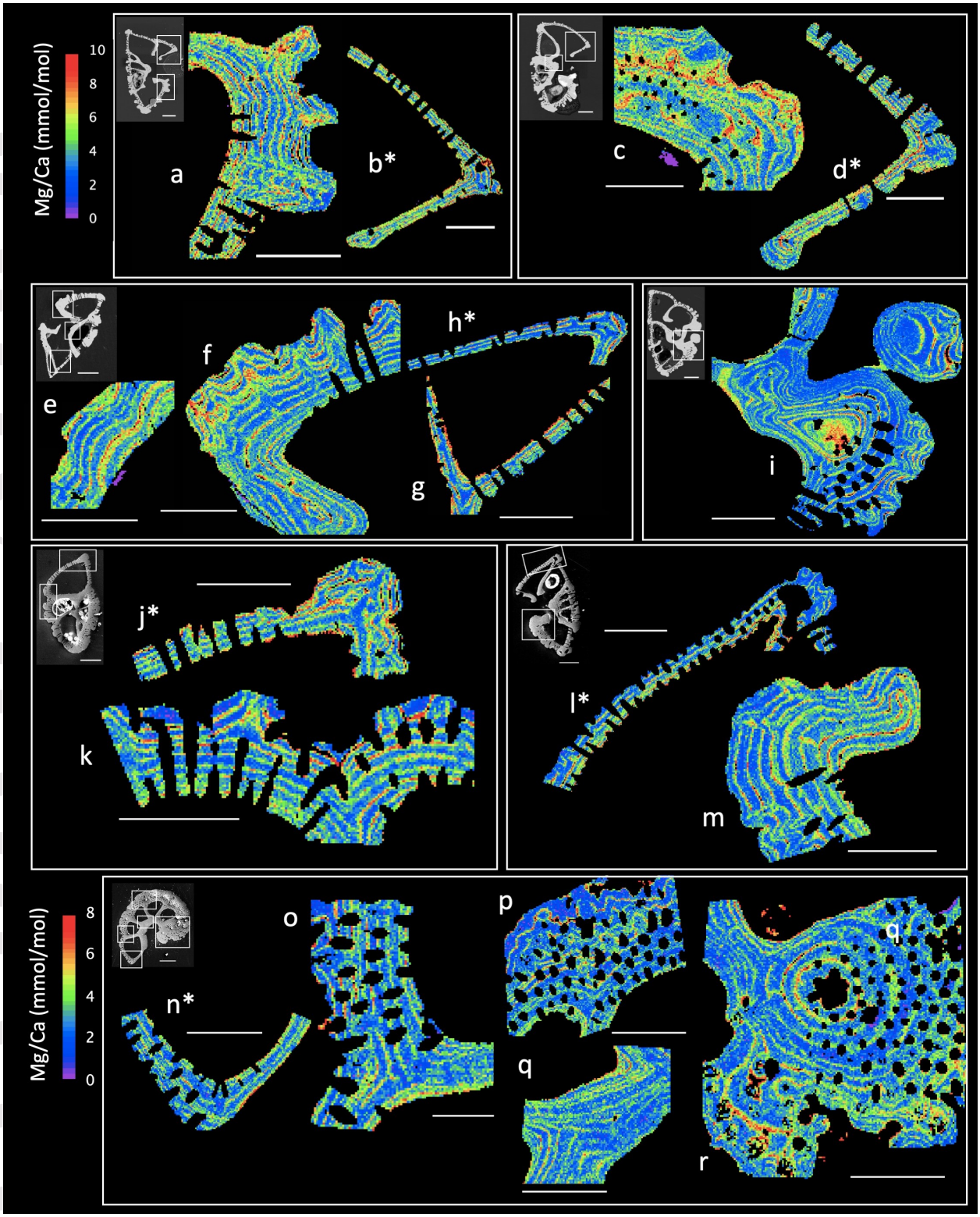

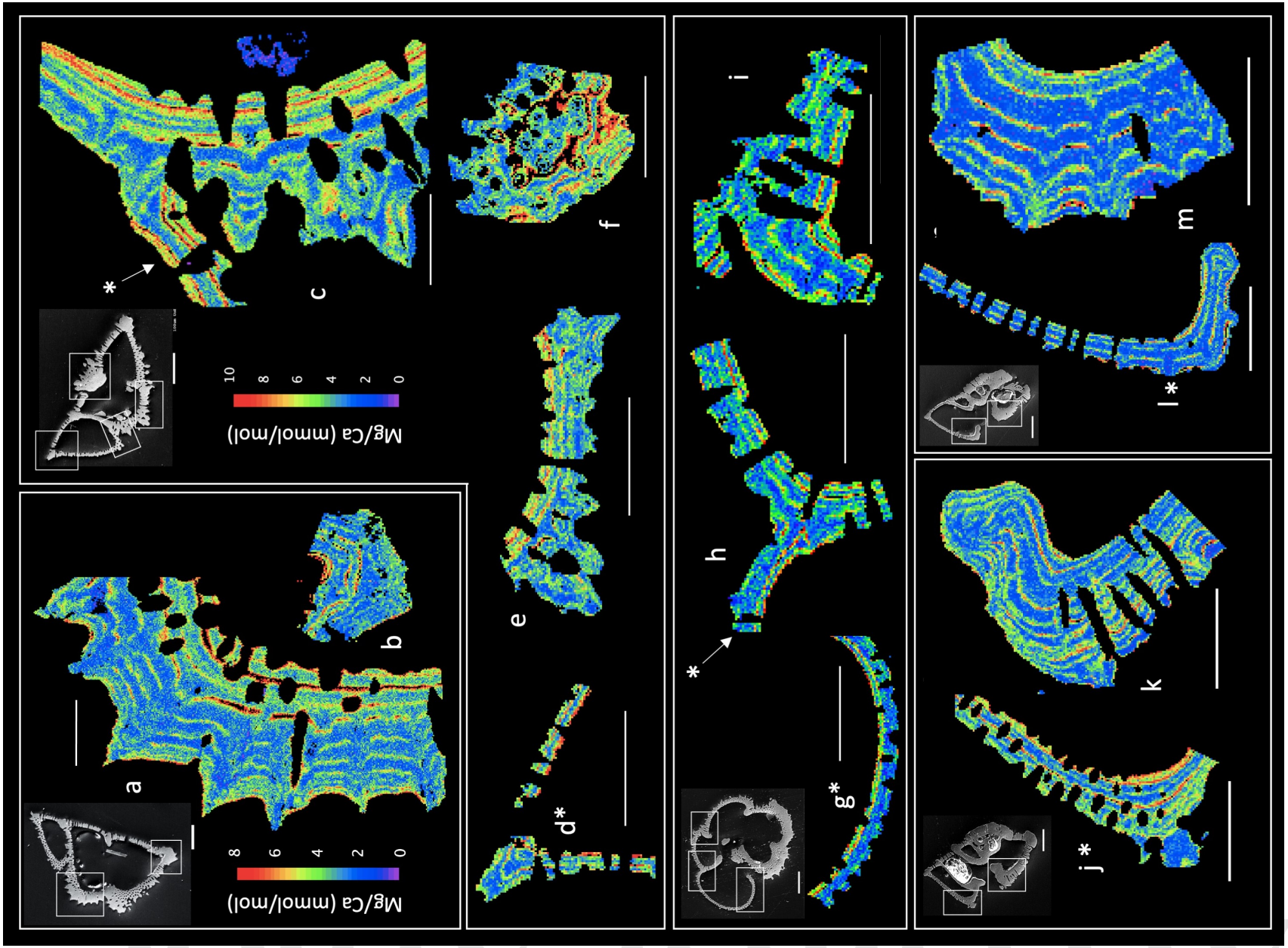

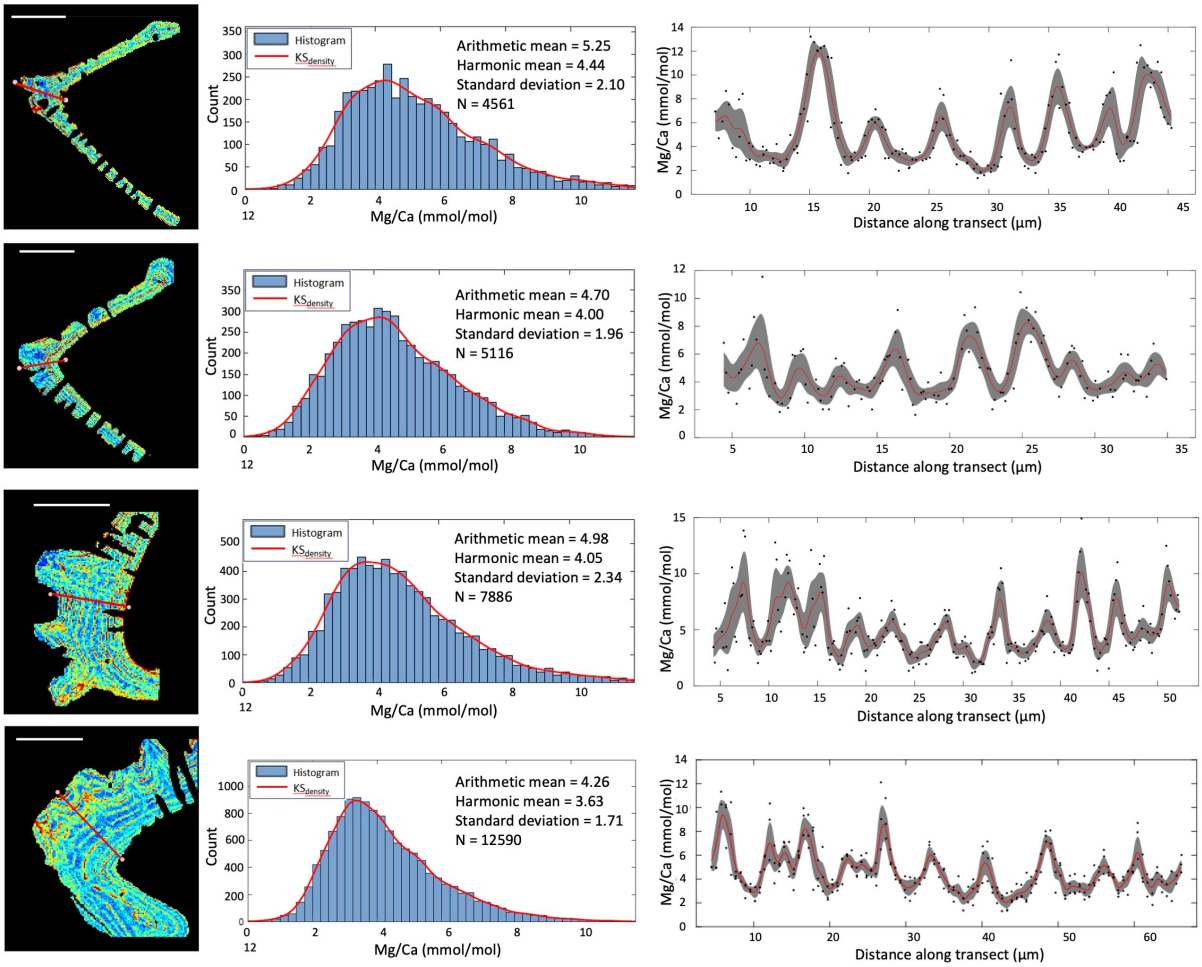

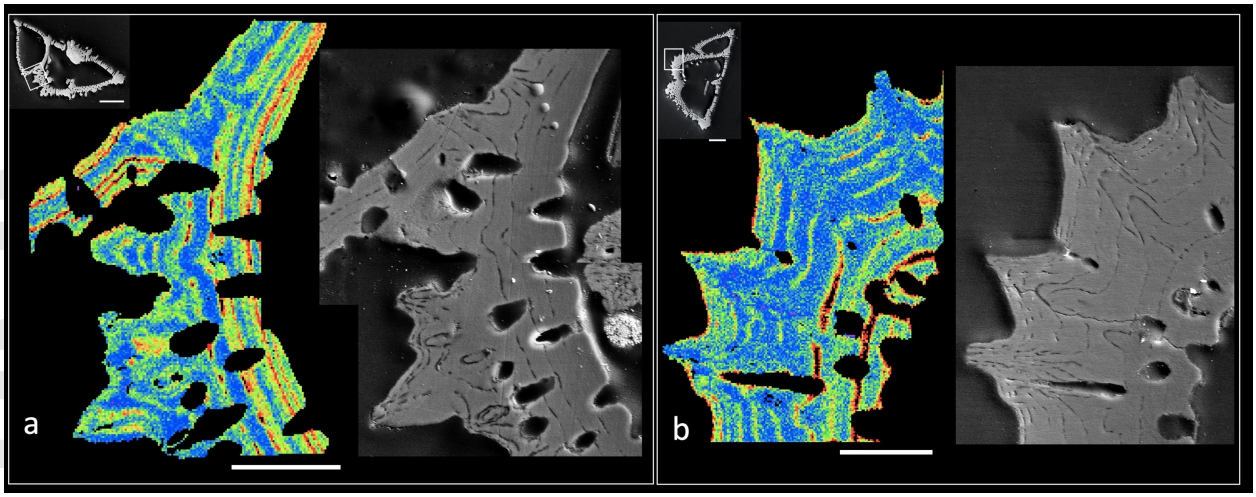

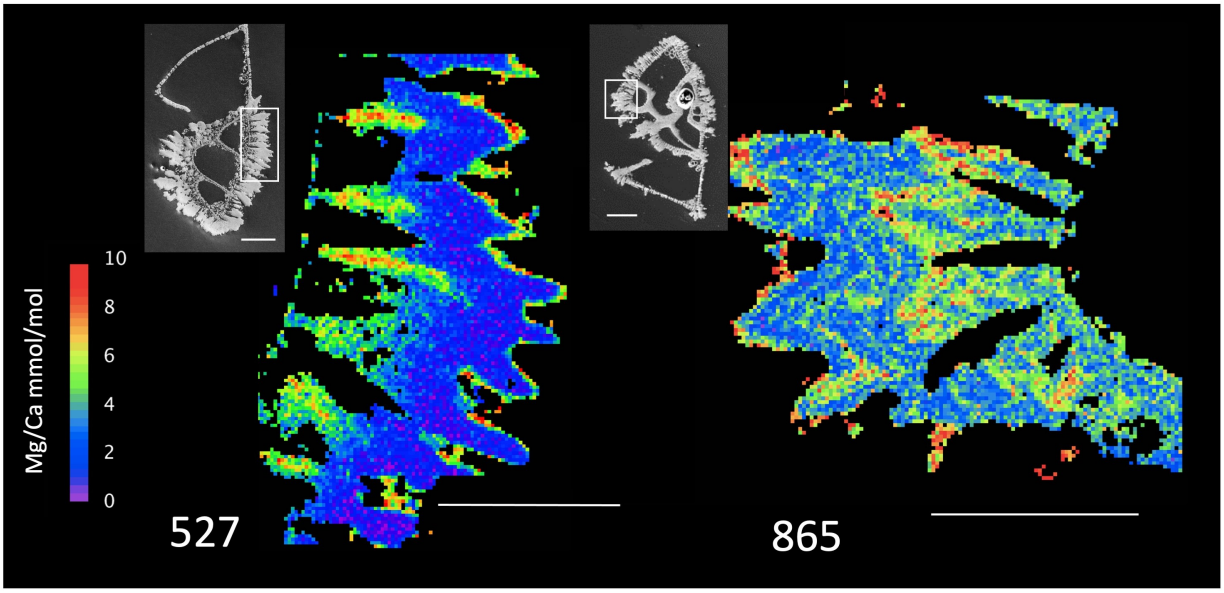

	Site location	Modern water depth (m)	Paleolatitude *	Burial depth (mbsf)	Sediment type	EPMA Mg/Ca map average (mmol/mol)	ICP-MS Mg/Ca bulk (mmol/mol)
ODP Site 527 (527* 18R-4 76-80 cm)	Walvis Ridge, 28°02.49'S, 01°45.80'E	4428	28°S	~161	Nannofossil ooze (~90% carbonate)	2.82 ± 1.92 (1 s.d.)	3.24 ± 0.29 (1 s.d.)
ODP Site 865 (865B 9H-6 0-4 cm)	Allison Guyot, NE Pacific, 18°26.415'N, 179°33.349'W	1516	12°N	~84	Foraminifera nannofossil ooze (>90% carbonate)	4.23 ± 1.76 (1 s.d.)	4.77 ± 0.17 (1 s.d.)